*Journal of Applied Fluid Mechanics*, Vol. 9, No. 3, pp. 1349-1357, 2016.
Available online at www.jafmonline.net, ISSN 1735-3572, EISSN 1735-3645.
DOI: 10.18869/acadpub.jafm.68.228.24509

# Investigation of Particles Statistics in large Eddy Simulated Turbulent Channel Flow using Generalized lattice Boltzmann Method

M. Samari Kermani[1] , S. Jafari[1†], M. Salmanzadeh[1] and M. Rahnama[1]

[1] *Mechanical Engineering Department, Shahid Bahonar University of Kerman, Kerman, Iran*
[2] *Petrolium Engineering Department, Shahid Bahonar University of Kerman, Kerman, Iran*

†*Corresponding Author Email: jafari@uk.ac.ir*

(Received January 13, 2015; accepted June 4, 2015)

## ABSTRACT

The interaction of spherical solid particles with turbulent eddies in a 3-D turbulent channel flow with friction Reynolds number $\mathrm{Re}=\frac{u_\tau * H}{\nu}=180$ was studied. A generalized lattice Boltzmann equation (GLBE) was used for computation of instantaneous turbulent flow field for which large eddy simulation (LES) was employed. The sub-grid-scale (SGS) turbulence effects were simulated through a shear-improved Smagorinsky model (SISM), which can predict turbulent near wall region without any wall function. Statistical properties of particles behavior such as root mean square (RMS) velocities were studied as a function of dimensionless particle relaxation time ( $\tau^+$ ) by using a Lagrangian approach. Combination of SISM in GLBE with particle tracking analysis in turbulent channel flow is novelty of the present work. Both GLBE and SISM solve the flow field equations locally. This is an advantage of this method and makes it easy implementing**.** Comparison of the present results with previous available data indicated that SISM in GLBE is a reliable method for simulation of turbulent flows which is a key point to predict particles behavior correctly.

**Key words:** Generalized lattice Boltzmann equation, Large eddy simulation, Particle tracking, Fluid mean velocity, Fluid root-mean-square (RMS) fluctuation velocity, Particle mean velocity, Particle root-mean-square (RMS) fluctuation velocity.

## NOMENCLATURE

| | | | |
|---|---|---|---|
| $C_c$ | Stokes- Cunningham slip correction factor | $u_\tau$ | shear velocity |
| $C_D$ | drag coefficient | $^F u^+_{RMS}$ | fluid dimensionless stream-wise RMS velocity |
| $C_s$ | Smagorinsky constant | $^F v^+_{RMS}$ | fluid dimensionless span-wise RMS velocity |
| d | particle's diameter | $^F w^+_{RMS}$ | fluid dimensionless normal RMS velocity |
| $dp/dx$ | pressure gradient | $^F u^+_{MEAN}$ | fluid dimensionless mean stream-wise velocity |
| $\vec{e_\alpha}$ | velocity vector in $\alpha$ direction | $^P u^+_{RMS}$ | particle dimensionless stream-wise RMS velocity |
| $f$ | velocity distribution function | $^p v^+_{RMS}$ | particle dimensionless span-wise RMS velocity |
| $\vec{F}$ | external force vector of flow domain | $^P u^+_{MEAN}$ | particle dimensionless mean stream-wise velocity |
| $g$ | gravity acceleration | $^P v^+_{MEAN}$ | particle dimensionless mean span-wise velocity |
| $g^+$ | Dimensionless gravity acceleration | | |
| $H$ | channel half width | | |
| $m$ | moments vector | | |
| $m^{eq}$ | equilibrium moments vector | | |
| $m_p$ | particle's mass | | |
| $M$ | transformation matrix of velocity | | |

| | | | |
|---|---|---|---|
| Re | flow friction Reynolds number | $^{P}w^{+}_{RMS}$ | particle dimensionless normal RMS velocity |
| $\mathrm{Re}_P$ | particle Reynolds number | $z^+$ | dimensionless distance from the lower wall |
| $s$ | particle to fluid density ratio | $\alpha$ | characteristic directions presented by the LBM model |
| S(x, t) | Shear at position x and time t | $\Delta$ | grid filter width |
| $\lvert S_\Delta(x,t)\rvert$ | magnitude of instantaneous resolved rate of strain | $\Delta x$ | local grid spacing in $x$ direction |
| $\mathbf{S}(\vec{X},t)$ | Source term vector | $\lambda$ | molecular mean free path of the gas |
| $\hat{s}$ | diagonal matrix of relaxation rates | $\nu$ | fluid kinematic viscosity |
| $t$ | time | $\nu_T$ | eddy viscosity |
| $t^+$ | Non-dimensional time | $\rho$ | density |
| $\vec{U}$ | fluid velocity vector | $\tau$ | Particle relaxation time |
| $u_i$ | fluid velocity in i direction | $\tau^+$ | dimensionless particle relaxation time |
| $u_i^p$ | particle velocity in i direction | | |

## 1. INTRODUCTION

Particle-laden turbulent flows have a wide range of applications in industrial and engineering fields. Usually turbulent flows are consisting of multiple phases and include suspended particles. Apparent examples are cooling air flow of micro-electronic devices or conveying the concentrate particles by air in mineral and cement factories. Also, particulate flows occur in indoor air and outdoor air filtration systems, industrial copper melting furnaces, sprays, drug delivery devices and mechanical polishing instruments. Sediment transport in rivers and dust storms are other examples that need the knowledge aerosol science and multiphase flows.

In order to predict particles transportation correctly, instantaneous fluid velocity components have to be evaluated carefully and economically. Direct numerical simulation (DNS) of fluid flow in which Navier-Stokes equations are solved without any model presents the most acceptable results. However, its high computational cost makes it inapplicable for large Reynolds number (RE) flows. Reynolds averaged Navier-Stokes (RANS) models contain empirical parameters and are not so efficient to predict underlying structure of turbulence and instantaneous velocity field. Large eddy simulation (LES) is an approach intermediate to the two previous methods. LES simulates the large scales that contain most of the kinetic energy of the flow, and then models the sub grid scales (SGS) which are problem independent and contain a small fraction of energy. An important advantage of LES is its ability to approach DNS with improved computational facilities and/or more accurate SGS modeling (Jafari and Rahnama, 2011). Fernandino, Beronov, and Ytrehus (2009) performed an LES of free surface duct flow using LBM in which Smagorinsky subgrid scale (SGS) model was used. Their results showed that the simple SGS model could be used as a possible tool for the simulation of free surface duct flow. Premnath *et al*. (2009a) presented a framework for LES using GLBE with a forcing term, for wall-bounded flows. They emphasized the numerical stability of their method even on a coarse grid and its ability to be used in a variable-resolution multiblock approach. They assessed their method for fully developed channel flow and shear-driven flow in a cubical cavity. Channel flow studies were reported for a. Reynolds number of 183.6 based on friction velocity and channel half-width. Their results showed reasonable agreement with DNS and experimental data. Sajjadi *et al*. (2011) investigated natural convection flow in large eddy simulated turbulent flow using LBM. They studied the results of high Rayleigh numbers between $10^6$ and $10^9$ for air with Pr=0.71. Their results proved that large eddy turbulence model by LBM is in acceptable agreement with other verifications of such a flow.

A number of studies that employed a Lagrangian model to track particles in wall-bounded turbulent flows have been reported. Pedinotti *et al*. (1992) performed DNS in wall bounded turbulent flows and demonstrated the accumulation of inertial particles in the near wall region. Wang and Squires (1996) used LES method to investigate particle transportation, and particle turbulent intensity relative to the fluid. They also generated the SGS fluctuation velocities using random numbers sampled from a Gaussian distribution. Rouson and Eaton (1994, 2001) studied particles behavior in a turbulent channel flow by performing direct numerical simulation of flow field and discussed about particles mean and fluctuating velocities. They also illustrated the preferential concentration of particles in low speed streak regions. Nasr, Ahmadi, and Mclaughlin (2009) evaluated the flow field by implementing DNS of Navier-Stokes equations via a pseudo-spectral method, while tracked the particles in a turbulent channel flow by a Lagrangian approach. In their work, the effects of inter-particle

collisions, two-way coupling, and particle aerodynamic interaction on both gas and solid phase fluctuations were examined. Salmanzadeh *et al*. (2010) developed a SGS model to study the effect of SGS turbulence fluctuations on particles root-mean-square fluctuation velocities, and also dispersion and deposition processes. They showed that SGS fluctuations increase the deposition rate. Salmanzadeh *et al*. (2012) modeled the effect of thermal plume adjacent to the body on particle transport and showed that temperature gradient made an important role in transporting $1\mu m$ particles. Jung *et al*. (2013) simulated turbulent duct flow using lattice Boltzmann method, and then allowed inertial particles to be tracked through a static probability density field distribution. Their results suggested that accurate particle tracking is feasible given a suitable probability field. Samari *et al*. (2014) investigated particles deposition in turbulent channel flow using generalized lattice Boltzmann method.

In the present study, application of SISM in large eddy simulation of turbulent flow is used through a generalized lattice Boltzmann method (GLBM). In fact LBM was used because of its important features that distinguish it from other numerical methods. First, the convention operator of the LBM in velocity space is linear. Second, the pressure in LBM is calculated using an equation of state. And third, the LBM utilizes minimal set of velocities in phase space. Since both GLBM and SISM do local calculations to solve the fluid velocity field, the method is easy coding and cost effective. Particles were tracked as they move under the influence of drag, buoyancy, gravitational, and Brownian forces. Results of the present one-way coupled simulations were in an acceptable agreement with previous data of Rouson and Eaton (1994).

## 2.1 Fluid Flow

In order to simulate flow field using lattice Boltzmann Method (LBM), fictitious particles groups i.e. distribution functions perform consecutive propagation and collision processes over a discrete lattice mesh. An important parameter in LBM computation is the relaxation time in the modeling of the collision step that distribution functions relax toward their local equilibrium values and in streaming process they move along the characteristic directions given by the LBM model (Succi 2001; Aidun and Clausen 2010). A single relaxation time (SRT) LBM has been used for a wide range of fluid flow problem because of its simplicity (Qian *et al*. 1992; Djenidi 2008). However, numerical instability of SRT along with the lack of proper mechanism for dissipation of small-scale unphysical oscillations arising from the kinetic model where the main reasons of shifting toward multiple relaxation time (MRT) LBM which is sometimes called generalized Lattice Boltzmann equation (GLBE). While LBM performs both collision and streaming steps in usual particle velocity space, generalized Lattice Boltzmann method (GLBM) computes the collisions in moment space and the streaming process is performed in the usual particle velocity space. Since GLBM uses multiple relaxation times, it shows a significant improvement in the numerical stability as compared SRT LBM model (Lallemand and Luo, 2000; Humières *et al*. 2002). This characteristic makes the GLBM suitable for simulation of turbulent flows. The effect of external forces can also be considered in an additional force term. Generalized Lattice Boltzmann equation (GLBE) with forcing term is written in the form of:

$$f(\overrightarrow{X}+\vec{e}\delta t, t+\delta t) = f(\overrightarrow{X}, t) - M^{-1}.\hat{s}.[m-m^{eq}(\rho,\overrightarrow{U})](\vec{X},t) + M^{-1}.(I-\frac{1}{2}\hat{s}).\boldsymbol{S}(\overrightarrow{X},t) \quad (1)$$

as stated in Premnath *et al*. (2009a).

In the present study, D3Q19 model was used to simulate the flow field, so all the vectors in Eq. (1) have 19 components. The last term in Eq. (1) shows the effect of source terms in moment space which are functions of $\vec{F}$ and $\overrightarrow{U}$. Components of $\boldsymbol{S}(\vec{X},t)$, $\hat{s}$, $m$ and $m^{eq}$ are mentioned in Premnath *et al*. (2009a,b); and Pattison *et al*. (2009).

In D3Q19 model the macroscopic density and momentum on each lattice node are calculated from Eq. (1) and Eq. (2).

$$\rho = \sum_{\alpha=0}^{18} f_\alpha \quad (2)$$

$$\rho\vec{u} = \sum_{\alpha=1}^{18} \overrightarrow{e_\alpha} f_\alpha + \frac{1}{2}\vec{F}\delta_t \quad (3)$$

In matrix $\hat{S}$, the relaxation rates which correspond to hydrodynamic modes can be related to transport coefficients and modulated by eddy viscosity due to SGS model (Premnath *et al*. 2009a; Humières 2002; Yu *et al*. 2006) as: $s_1^{-1} = 0.5(9\xi+1)$, where $\xi$ is molecular bulk viscosity, and

$$s_9 = s_{11} = s_{13} = s_{14} = s_{19} = s_\nu \text{ with}$$

$$s_\nu^{-1} = 3\nu' + 0.5 = 3(\nu+\nu_T) + 0.5 \quad (4)$$

Other relaxation rates are indicated as: (Premnath *et al*. 2009a)

$$s_1 = 1.19,\ s_2 = s_{10} = s_{12} = 1.4,$$
$$s_4 = s_6 = s_8 = 1.2,$$
$$s_{16} = s_{17} = s_{18} = 1.98$$

Strain rate tensor components, used to model SGS turbulence, can be written in terms of non-equilibrium moments - $h^{neq}$. For instance:

$$S_{xx} \approx -\frac{1}{38\rho}\left[ s_1 h_1^{neq} + 19 s_9 h_9^{neq} \right] \tag{5}$$

$$h_\alpha^{neq} = m_\alpha - m_\alpha^{eq} + \frac{1}{2}\boldsymbol{S}_\alpha \tag{6}$$

Other components can be found in (Premnath *et al*. 2009a).

The magnitude of strain rate tensor can be calculated using Eq. (7).

$$|S| = \sqrt{2S_{ij}S_{ij}} = \sqrt{2\left[ S_{xx}^2 + S_{yy}^2 + S_{zz}^2 + 2(S_{xy}^2 + S_{yz}^2 + S_{xz}^2) \right]} \tag{7}$$

### 2.1.1 Calculation of Eddy Viscosity with Shera- Improved Smagorinsky Model

In order to model turbulence in lattice Boltzmann method, a varying relaxation toward equilibrium, i.e. $\hat{s}$ in Eq. (1), was used. For computing sub-grid scale stresses, shear-improved Smagorinsky model was implemented (Leveque *et al*. 2007). In this model SGS eddy viscosity has two types of intractions. The one between the mean velocity gradient and the resolved fluctuating velocities, and the other one among the resolved fluctuating velocities themselves. The former is related to the large-scale distortion, while the latter is associated with the Kolmogorov's energy cascade (Jafari and Rahnama, 2011). For evaluation of SGS eddy viscosity, the magnitude of the shear should be subtracted from the instantaneous resolved rate of strain as in Eq. (8). This improvement accounts for the large- scale distortion in regions of strong shear like near a solid boundary, and also allows us to recover the standard Smagorinsky model in regions of locally homogeneous and isotropic turbulence (at grid scale). The SISM does not use any adjustable parameter, a damping function or any kind of dynamic adjustment. Results concerning a plane-channel flow (Leveque *et al*. 2007) and a backward-facingstep flow (Toschi *et al*. 2006) have shown good predictive capacity of this model, essentially equivalent to thedynamic Smagorinsky model (Germano *et al*. 1991), but with a computational cost and manageability comparable to the original Smagorinsky model.

$$\nu_T^{SISM}(x,t) = (C_S\Delta)^2\left(|S_\Delta(x,t)| - S(x,t)\right) \tag{8}$$

In this equation $C_S$=0.18 for homogeneous and isotropic turbulence and $\Delta = (\Delta x \Delta y \Delta z)^{\frac{1}{3}}$. Since the flow is assumed to be well enough resolved in the direction of the shear, then $S(x,t) \approx \left|\left\langle S_\Delta(x,t)\right\rangle\right|$ (Jafari and Rahnama 2011).

In the present study, spatial averaging over homogeneous directions in the channel (x and y directions) was used to compute $\left|\left\langle S_\Delta(x,t)\right\rangle\right|$ and Eq. (7) was employed for calculation of rate of strain. So $\nu_T^{SISM}$ obtained from Eq. (9) and was used as eddy viscosity in this turbulent flow.

$$\nu_T^{SISM}(x,t) = (C_S\Delta)^2\left(|S| - \left|\left\langle S_\Delta(\vec{X},t)\right\rangle\right|\right) \tag{9}$$

The total viscosity which is sum of the physical and the eddy viscosity is substituted in Eq. (4).

## 2.2 Computational Domain

The selected channel has dimensions of $6H \times 3H \times 2H$ in stream-wise, span-wise and cross sectional directions, respectively. The Reynolds number based on the shear velocity and channel half width is 180 for which previous DNS data exists. The flow is bounded from top and bottom by two no-slip walls. Owing to presence of fully developed flow in stream- wise direction and homogeneity in span-wise direction, periodic boundary condition was selected for these two directions (Succi, 2001).

A uniform grid was used for present simulation, and the computational domain was discretized into $240 \times 120 \times 80$ nodes in stream-wise, span-wise and wall directions, respectively. This corresponds to a mesh with resolution of 4.5 wall units in each direction. Because of using half-way bounce-back scheme for implementation of wall boundary condition, the first grid point is located at a distance of 2.25 wall units from the wall. The driving force in the present channel flow is pressure gradient in flow direction and can be related to wall shear velocity $\tau_w$ , and $u_\tau$ through:

$$\vec{F} = -\frac{dp}{dx}\vec{i} = \frac{\tau_w}{H}\vec{i} = \frac{\rho u_\tau^2}{H}\vec{i} \tag{10}$$

## 2.3 Particle Discrete Phase

Here the Lagrangian approach was selected to solve the dispersed phase whereas the carrier phase is treated via an Eulerian approach as explained in previous sections. The governing equations of motion are given by:

$$\frac{dU_i^p}{dt} = \frac{1}{\tau}\frac{C_D\,\mathrm{Re}_p}{24}(U_i - U_i^p) + (1 - \frac{1}{\mathbf{s}})g_i + n_i(t). \tag{11}$$

$$dX_i/dt = U_i^p. \tag{12}$$

Where

$$\tau = \mathbf{s}d^2 C_C / 18\nu. \tag{13}$$

$$C_C = 1 + \frac{2\lambda}{d}(1.257 + 0.4\exp(-1.1d/2\lambda)). \tag{14}$$

$$C_D = \begin{cases} \dfrac{24}{\mathrm{Re}_p} & \mathrm{Re}_p \prec 1 \\ \dfrac{24}{\mathrm{Re}_p}(1 + 0.15\mathrm{Re}_p^{0.687}) & 1 \prec \mathrm{Re}_p \prec 400 \end{cases} \tag{15}$$

$$\mathrm{Re}_p = d\left|U_i - U_i^p\right|/\nu. \qquad (16)$$

The first term on the right hand side of Eq. (11), is the Stokes drag force due to particle and fluid relative slip. The second term represents the buoyancy effect. And, the last term depicts the Brownian force per unit mass that shows the impact of fluid molecules on the particle and is modeled as a Gaussian white noise random process. The Brownian force is described in detail by Ounis *et al*. (1993) and therefore is not presented here.

The effect of turbulence is considered on transport and dispersion of particles via using instantaneous fluid velocity field in particles equation of motion. In order to solve Eq. (11), fluid velocity in particle location is evaluated by a volume averaged interpolation scheme (Salmanzadeh *et al*. 2010).

## 3. RESULTS

### 3.1 Fluid Flow Velocity Field

In order to make sure about the accuracy of fluid velocity field, root-mean-square (RMS) fluctuation velocities became non- dimensional by $u_\tau$ and they were compared with RMS velocities obtained from DNS (Kim *et al*. 1987) and GLBE with Smagorinsky model (Premnath *et al*. 2009a). The results show a reasonable agreement and are shown in Fig 1.

To show a grid independent study and before settling on a $240\times120\times40$ grid with mesh resolution of 4.5 wall units, non-dimensional fluid RMS velocities were calculated for different grid resolutions, and the profiles are shown in Fig 2. Although a coarse mesh with resolution of 6 was used on a $180\times90\times30$ grid, the comparison between these resolutions shows an acceptable agreement. In order to save mesh resolution and obtain accurate results, it is clear that a finer grid have to be used if the flow friction Reynolds number (Re) increases.

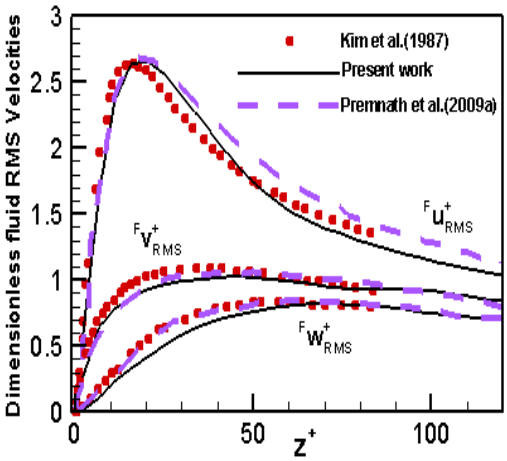


**Fig. 1. Fluid fluctuation velocities.**

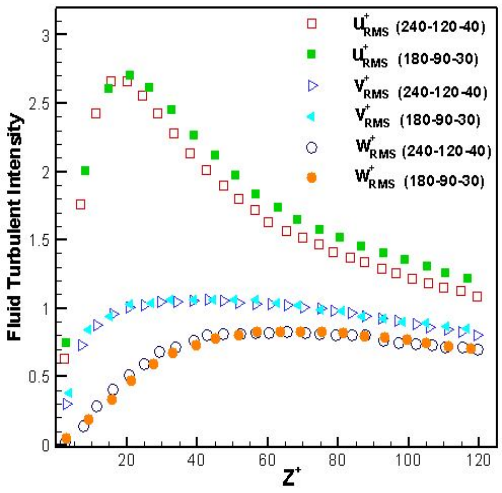


**Fig. 2. Fluid RMS fluctuation velocity profiles for different grid resolutions.**

### 3.2 Particles Velocity Statistics

After reaching the flow field to a statistically steady state, 200,000 particles were randomly distributed throughout the channel, and their initial velocities were set equal to fluid velocity at particles' locations. To check the accuracy of the calculations, at first simulations were done for particles with the same relaxation times as those used in DNS of Rouson and Eaton (1994). Results of fluid and particles mean and RMS velocities are presented in Fig. 3, Fig. 4, and Fig. 5 for different values of $\tau^+$. There is reasonable agreement between present simulation results and previous data. The difference is may be due to using different simulation methods i.e. DNS and LES and also different grid resolution in these two works. Why the figures show such trends for vrious values of $\tau^+$, is discussed in following sections.

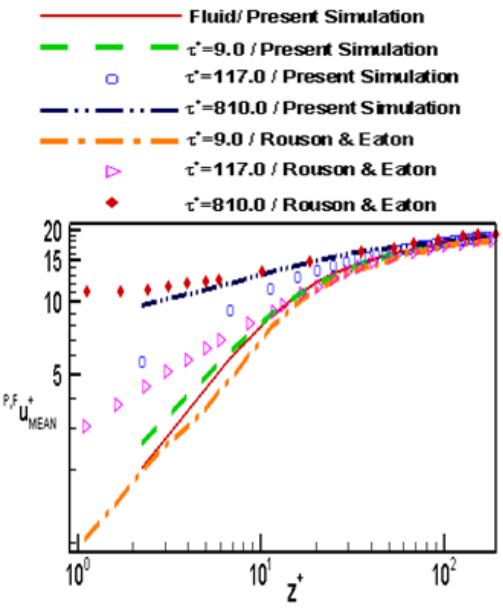


**Fig. 3. Mean stream-wise fluid and particle velocities vs. the distance from the wall.**

Simulations were also done by tracking and recording the velocity statistics of 200,000 particles with $\tau^+ = 0.0216$, $\tau^+ = 1.0$, $\tau^+ = 4.0$, $\tau^+ = 10.0$, $\tau^+ = 20.0$, and $\tau^+ = 40.0$ for $t^+ = \frac{t^* u_\tau^2}{\nu} = 1000$ and air flow at $T = 288\ K$, $\nu = 1.5\times10^{-5}\ \frac{m^2}{s}$, $u_\tau = 0.36\ m/s$ and $\mathbf{s} = 2000$. It is note- worthy that it is a one-way coupled simulation that the effect of particle feedback force on the flow is negligible. It is showed that this approach is valid for volume fractions less than $10^{-6}$ (Elghobashi and Truesdell, 1993). Here the maximum volume fraction is about $5.4\times10^{-10}$ related to particles with $\tau^+ = 40.0$. This volume fraction of the dispersed phase is small enough such that particle collisions are negligible and properties of the carrier flow are not modified. This small concentration allows the continuum assumption to be invoked.

The dispersed phase statistics were obtained by averaging over x-y planes and time. Fig. 6 shows mean stream-wise particle velocity profiles versus dimensionless distance from the wall, $z^+$.

$$z^+ = \frac{z^* u_\tau}{\nu} \qquad (17)$$

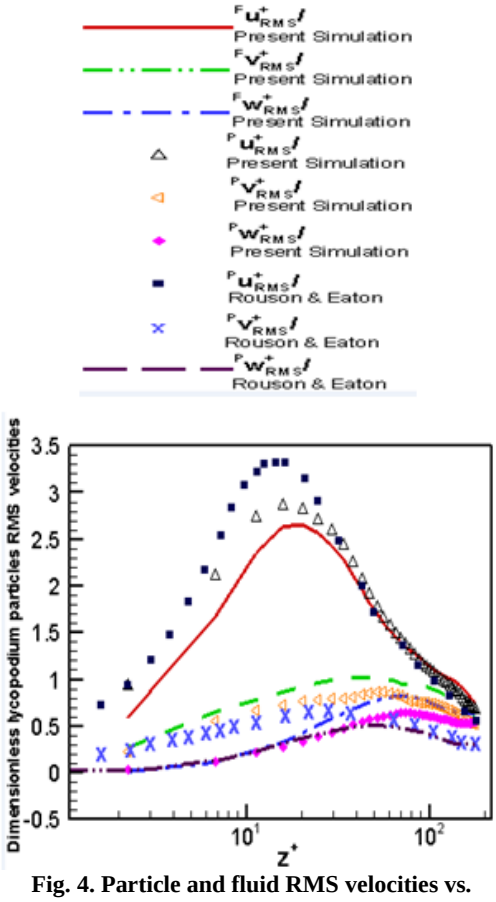


**Fig. 4. Particle and fluid RMS velocities vs. distance from the wall** $(\tau^+ = 9.0)$ **.**

It is seen that particles with small $\tau^+$ ($\tau^+ = 0.0216$ and $\tau^+ = 1.0$) are flow tracers. As the particles become inertia ($\tau^+ \geq 20.0$) they begin to lead the flow especially in wall region, $z^+ \prec 30.0$. This phenomenon is a part due to stream-wise gravitational acceleration, and a part due to migration of these large and fast speed particles from channel core into the wall region. It is seen particles with $\tau^+ = 4.0$ and $\tau^+ = 10.0$ slightly lag the flow where $10.0 \prec z^+ \prec 30.0$. This result is may be because of preferential concentration of these particles in low-speed streaks as Rouson and Eaton (1994) reported first**.**

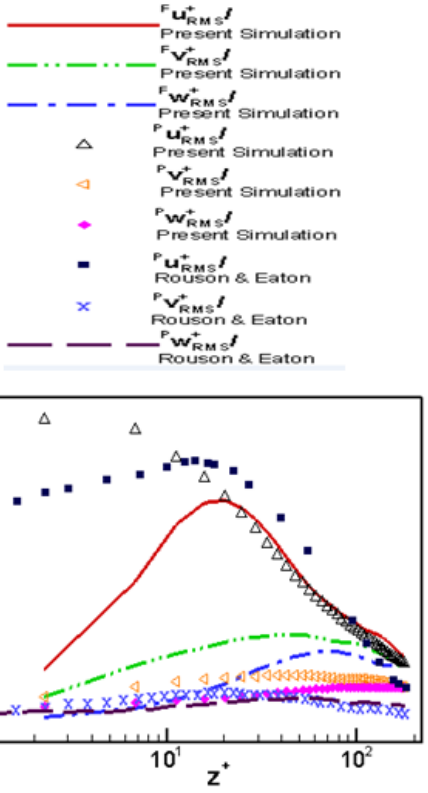


**Fig. 5. Particle and fluid RMS velocities vs. distance from the wall** $(\tau^+ = 117.0)$ **.**

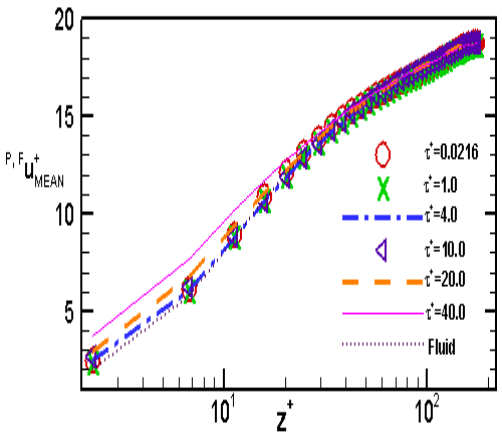


**Fig. 6. Mean stream-wise particle velocity vs. distance from the wall.**

Particle stream-wise RMS velocities are shown in Fig.7. It is illustrated that by increasing particles inertia, higher stream-wise fluctuation velocities are seen especially in wall region. This fact is related to existence of two different particle categories near the wall. One which contains low velocity particles that have already been in this region, and the other one that contains high velocity particles migrated from channel core to this region. These large, migrated particles are inertia, they show less responsiveness to the flow and keep their momentum for a long time; therefore, there is a wide range of stream-wise velocities in the wall region and as a result the particle stream-wise fluctuating velocity increases. In $z^+ \geq 20.0$ particles with different $\tau^+$ values which are at the same distance from the wall have almost the same stream-wise RMS velocities;
Since, these particles are fast speed and their mean stream-wise velocities show no large normal gradient (Fig. 6); Thus, their migration between layers do not change RMS velocities considerably.

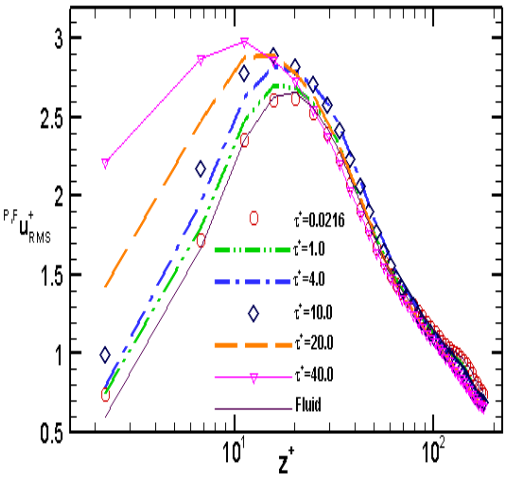


**Fig. 7. Particle stream-wise fluctuation velocity vs. the distance from the wall.**

As the presented results in Fig. 8 shows, particles span-wise turbulent intensity has a decreasing trend by increasing $\tau^+$ values owing to less obedience of inertial particles from turbulent eddies. Also as the particle relaxation time increases, it may be seen that the particle turbulent intensities become larger than the fluid in the stream-wise direction, but smaller in span-wise direction.

It is seen that for inertia particles the stream-wise fluctuating velocity increases while the span-wise turbulent intensities decreases. Since, particle span-wise velocity has a uniform zero-mean velocity in the whole channel, while there is a gradient for the stream-wise particle velocity. In fact, this velocity gradient causes the migrated particles to make two different particle categories near the wall.

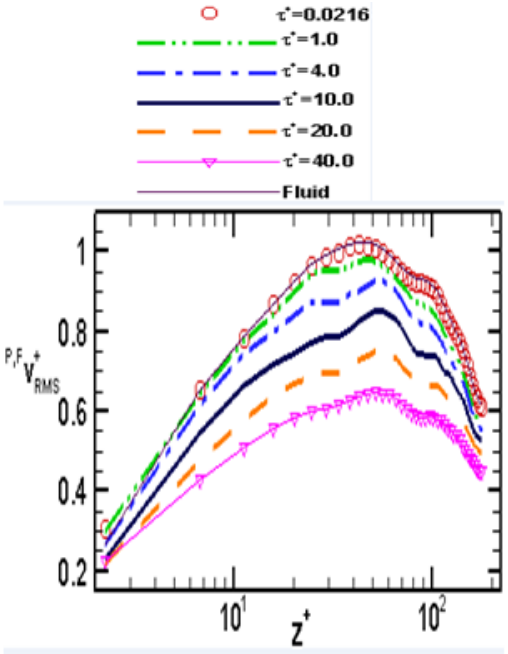


**Fig. 8. Particle span-wise fluctuation velocity vs. distance from the wall.**

Figure 9 shows the variation of RMS velocities of particles in wall direction for different non-dimensional relaxation times. This variation reveals that by increasing $\tau^+$ values in near wall region ($z^+ \prec 10.0$), where particles have a large mean normal velocity gradient i.e. the mean normal velocity of particles in different layers differ a lot from each other (Fig. 10), normal RMS velocities increase due to particles flux toward the wall. However, for $z^+ \succ 10.0$ where the gradient is not as large as in wall region, as $\tau^+$ increases, less responsiveness of the particles from the flow becomes more apparent. Therefore, the normal turbulent intensities decrease.

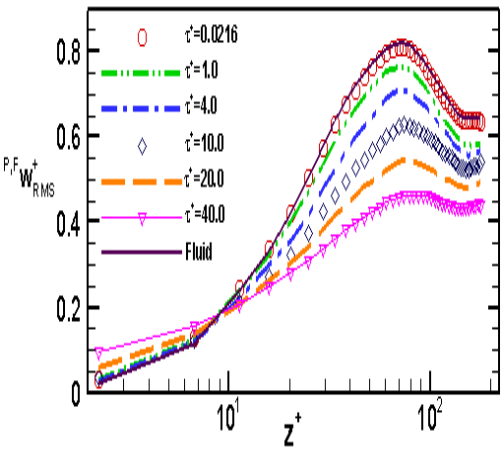


**Fig. 9. Particle normal fluctuation velocity vs. distance from the wall.**

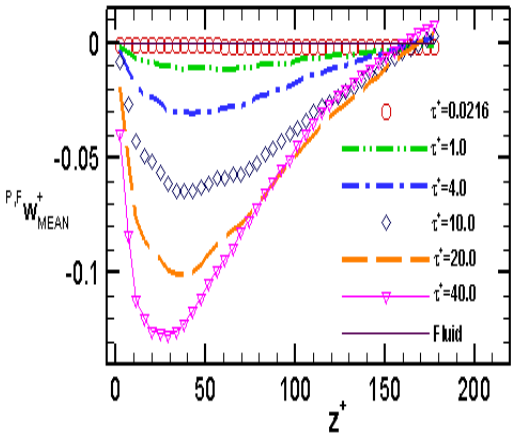


**Fig. 10. Mean normal particle velocity vs. distance from the wall.**

Figure 11 shows the reason of using non-linear drag coefficient for this particle-laden turbulent channel flow. It is observed that as particles become more inertial, their Reynolds number becomes greater. Also for all different values of $\tau^+$, $\mathrm{Re}_p$ gets its maximum value in wall region, where $\left|u_i - u_i^p\right|$ has a large value.

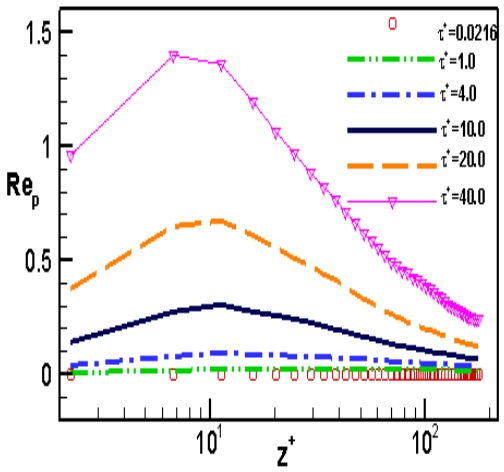


**Fig. 11. Particle Reynolds number vs. distance from the wall.**

## 4. CONCLUSION

Particles' statistics in large eddy simulated turbulent channel flow with $\mathrm{Re}=180$ were studied. Fluid flow velocity field was simulated using a generalized lattice Boltzmann method. And, SGS turbulence effects were modeled by SISM. Particle transport was studied using Lagrangian approach. Measured statistical properties of particles' velocities were compared with available DNS data, and reasonable agreement was demonstrated. Following conclusions can also be derived from the results.

Both GLBM and SISM solve the fluid velocity field locally. This property made the code easy implementing.

The GLBE with SISM is capable of capturing turbulent channel flow structures. It has the ability to predict instantaneous fluid velocity field correctly, which is a key point for particles' accurate behavior.

Statistics of particles movement simulated with good precision with this simulated flow field by LBM.

The followings could also be deduced from particles' simulation results:

As $\tau^+$ increases, mean stream-wise particle velocity increases.

By increasing $\tau^+$ values, stream-wise RMS velocity of particles in near wall region $(z^+ \prec 20.0)$ increases, while stream-wise RMS velocity of particles far from the wall $(z^+ \geq 20.0)$ nearly remains unchanged.

By increasing $\tau^+$ values, particle span-wise fluctuation velocity decreases.

As $\tau^+$ increases, mean normal particle velocity toward the wall increases.

By growing $\tau^+$ values, particle normal fluctuation velocity is increased in $z^+ \prec 10.0$, while it is decreased in $z^+ \succ 10.0$.

By increasing $\tau^+$ values, particles Reynolds number in stream-wise direction increases.

Particles Reynolds number gets its maximum in near wall region.

## REFERENCES

Aidun, C. K. and J. R. Clausen (2010). Lattice-Boltzmann Method for Complex Flows. *Annu. Rev. Fluid Mech 42, 439-472.*

Djenidi, L. (2008). Structure of a turbulent crossbar near-wake studied by means of Lattice Boltzmann simulation. *Physical Review. E, 77(3), 036310–036312.*

Elghobashi, S. and G. S. Truesdell (1993). On the two- way interaction of particle dispersion in a decaying isotropic turbulence. *Physics of Fluids, A 5, 1790-1801.*

Fernandino, M., K. Beronov and T. Ytrehus (2009). Large eddy simulation of turbulent open duct flow using a Lattice Boltzmann approach. Mathematics and Computers in Simulation 79, 1520–1526.

Germano, M., U. Piomelli, P. Moin and W. H. Cabot (1991). A dynamic subgrid- scale eddy-viscosity model. *Physics of Fluids, A 3, 1760–1765.*

Humières, D., I. Ginzburg, M. Krafczyk, P. Lallemand and L. S. Luo (2002). Multiple-relaxation time lattice Boltzmann models in

three dimensions. Philos. *Trans. R. Soc. London, Ser. A 360, 437-452.*

Jafari, S. and M. Rahnama (2011). Shear-improved Smagorinsky modeling of turbulent channel flow using generalized lattice Boltzmann equation. *Int. J. Numer. Methods Fluids 67, 700-712.*

Jung, S., D. J. Phares and A. R. Srinivasa (2013). A model for tracking inertial particles in a lattice Boltzmann turbulent flow simulation. *Int. J. Multiphase Flow 49, 1-7.*

Kermani, M. S., S. Jafari, M. Rahnama and M. Salmanzadeh (2014). Particle tracking in large eddy simulated channel flow using generalized lattice Boltzmann method. *Int. J. Particulate Science and Technology 32:4, 404-411.*

Kim, J., P. Moin and R. Moser (1987). Turbulence statistics in fully developed channel flow at low Reynolds number. *J. Fluid Mech 177, 133-166.*

Lallemand, P. and L. S. Luo (2000). Theory of the Lattice Boltzmann method: dispersion, dissipation, isotropy, Galilean invariance, and stability. *Physical Review E 61(6), 6546–6562.*

Leveque, E., F. Toschi, L. Shao and J. P. Bertoglio (2007). Shear-improved Smagorinsky model for large-eddy simulation of wall-bounded turbulent flows. *J. Fluid Mech 570, 491-502.*

Nasr, H., G. Ahmadi and J. B. Mclaughlin (2009). A DNS study of effects of particle-particle collisions and two-way coupling on particle deposition and phasic fluctuations. *J. Fluid Mech 640, 507-536.*

Ounis, H., G. Ahmadi and J. B. Mclaughlin (1993). Brownian particle deposition in a directly simulated turbulent channel flow. *Physics of Fluids A. 5, 6, 1427-1432.*

Pattison, M. J., K. N. Premnath and S. Banerjee (2009). Computation of turbulent flow and secondary motions in a square duct using a forced generalized lattice Boltzmann equation. *Physical Review. E 79(2), 026704-13.*

Pendinotti, S., G. Mariotti and S. Banerjee (1992). Direct numerical simulation of particle behavior in the wall region of turbulent flows in horizontal channels. *Int. J. Multiphase Flow 18, 927-941.*

Premnath, K. N., M. J. Pattison and S. Banerjee (2009a). Generalized lattice Boltzmann equation with forcing term for computation of wall bounded turbulent flows. *Physical Review. E 79(2), 026703-19.*

Premnath, K. N., M. J. Pattison and S. Banerjee (2009). Dynamic subgrid scale modeling of turbulent flows using lattice Boltzmann method. *Physica A 388, 2640-2658.*

Qian, Y. H., D. Humières and P. Lallemand (1992). Lattice BGK models for Navier–Stokes equation. *European Physics Letters 17(6), 479–484.*

Rouson, D. W. I. and J. K. Eaton (1994). Direct numerical simulation of particles interacting with a turbulent channel flow. *Proceedings of the 7th work-shop on two-phase flow predictions, edited by Sommerfeld M. Erlangen, Germany.*

Rouson, D. W. I. and J. K. Eaton (2001). On the preferential concentration of solid particles in turbulent channel flow. *J. Fluid Mech 428, 149-169.*

Sajjadi, H., M. Gorjim, S. F. Hosseinizadeh, G. R. Kefayati and D. D. Ganji (2011). Numerical analysis of turbulent natural convention in square cavity using large- eddy simulation in lattice Boltzmann method. *Iranian Journal of Science and Technology Transaction B-Engineering. 35(2), 133- 142.*

Salmanzadeh, M., Gh. Zahedi, G. Ahmadi, D. R. Marr and M. Glauser (2012). Computational modeling of effects of thermal plume adjacent to the body on the indoor airflow and particle transport. *J. Aerosol Science 53, 29–39.*

Salmanzadeh, M., M. Rahnama and G. Ahmadi (2010). Effect of sub-grid scales on large eddy simulation of particle deposition in a turbulent channel flow. *Aerosol Sci. Technol 44: 796-806.*

Succi, S. (2001). The lattice Boltzmann equation for fluid dynamics and beyond. *Oxford: Oxford University Press.*

Toschi, F., H. Kobayashi, U. Piomelli and G. Iaccarino (2006). Backward-facing step calculations using the shear improved smagorinsky model. *Proceedings of the Summer Program, Center for Turbulence Research, Stanford University, Stanford.*

Wang, Q. and K. D. Squires (1996). Large eddy simulation of particle-laden turbulent channel flow. *Physics of Fluids 8, 1207-1223.*

Yu, H., L. S. Luo and S. Girimaji (2006). LES of turbulent square jet flow using an MRT lattice Boltzmann model. *J. Comput. Fluids 35, 957-965.*